



ELSEVIER

Available online at [www.sciencedirect.com](http://www.sciencedirect.com)

SCIENCE @ DIRECT®

Journal of Computational Physics 212 (2006) 739–756

JOURNAL OF  
COMPUTATIONAL  
PHYSICS

[www.elsevier.com/locate/jcp](http://www.elsevier.com/locate/jcp)

# A weighted essentially non-oscillatory numerical scheme for a multi-class traffic flow model on an inhomogeneous highway

Peng Zhang <sup>a</sup>, S.C. Wong <sup>b,\*</sup>, Chi-Wang Shu <sup>c</sup>

<sup>a</sup> *Shanghai Institute of Applied Mathematics and Mechanics, Shanghai University, Shanghai, PR China*

<sup>b</sup> *Department of Civil Engineering, The University of Hong Kong, Hong Kong SAR, PR China*

<sup>c</sup> *Division of Applied Mathematics, Brown University, Providence, RI 02912, USA*

Received 16 May 2005; received in revised form 25 July 2005; accepted 26 July 2005

Available online 9 September 2005

---

## Abstract

As a new attempt to solve hyperbolic conservation laws with spatially varying fluxes, the weighted essentially non-oscillatory (WENO) method is applied to solve a multi-class traffic flow model for an inhomogeneous highway. The numerical scheme as well as an analytical study is based upon a modified equivalent system that is written in a “standard” hyperbolic conservation form. Numerical examples, which include the difficult traffic signal control problem, are used to demonstrate the effectiveness of the WENO scheme in which the results are in good agreement with the analytical counterparts.

© 2005 Elsevier Inc. All rights reserved.

*Keywords:* Multi-class traffic flow; Inhomogeneous highway; Non-strictly hyperbolic conservation laws; Spatially varying fluxes; WENO reconstruction

---

## 1. Introduction

In this paper, we extend a multi-class Lighthill–Whitham–Richards (LWR) traffic flow model [21,23,28] to deal with inhomogeneous road conditions. The variable road conditions are the number of lanes  $a(x)$  and the free flow (maximum) velocities  $\{v_{l,f}(x)\}_{l=1}^m$  of  $m$  types of vehicles. Let  $\rho_l(x,t)$  be the density per lane of the  $l$ th type, and let

---

\* Corresponding author. Tel.: +852 2859 1964; fax: +852 2559 5337.

E-mail address: [hhecwsc@hkucc.hku.hk](mailto:hhecwsc@hkucc.hku.hk) (S.C. Wong).

$$\rho(x, t) = \sum_{l=1}^m \rho_l(x, t)$$

be the total density per lane. The velocity of the  $l$ th type of vehicles is a function of  $\rho$ , which is denoted by  $v_l(\rho)$ . Furthermore, we assume that  $\{v_l\}_{l=1}^m$  are related by

$$v_l = b_l(x)v(\rho), \quad v'(\rho) < 0, \quad b_l(x) = v_{l,f}(x)/v_f, \quad v_f \equiv \max_x \max_{1 \leq l \leq m} (v_{l,f}(x)), \quad (1.1)$$

where the free flow velocity  $v_f$  is the maximum of the free flow velocities  $v_{l,f}(x)$  of the  $l$ th type at location  $x$ . Accordingly, the velocity differences between  $m$  vehicle types are reflected by the functions  $\{b_l(x)\}_{l=1}^m$  and  $0 \leq b_l(x) \leq 1$ .

The model equations are acquired from the mass conservation of  $m$  types of vehicles, which read

$$(a(x)\rho_l)_t + (a(x)\rho_l b_l(x)v(\rho))_x = 0, \quad 1 \leq l \leq m. \quad (1.2)$$

Eq. (1.2) is a natural extension of the so called multi-class LWR model that was proposed in [21] and studied in [23,28]. The present model reduces to that in [21,23,28] when  $a(x)$  and  $\{v_l\}_{l=1}^m$  are constants. We introduce the conservative solution variables  $u_l = a(x)\rho_l$ , the vector  $u = (u_1, \dots, u_m)^T$ , and the flux vector  $f = (f_1, \dots, f_m)^T$  with  $f_l = b_l u_l v(\Sigma u_l/a)$ . Accordingly, the model equations can be written as

$$u_t + f(u, \theta(x))_x = 0, \quad (1.3)$$

where the vector function  $\theta(x)$  represents all inhomogeneous factors on the road, namely,

$$\theta(x) = (a(x), b_1(x), \dots, b_m(x)).$$

In this traffic flow problem, each density  $\rho_l$  and the total density  $\rho$  are bounded by a jam density  $\rho_{\text{jam}}$ , and thus

$$u/a \in \bar{D}, \bar{D} = \left\{ u/a | \rho_l \geq 0, \quad l = 1, \dots, m; \quad \sum_{l=1}^m \rho_l \leq \rho_{\text{jam}} \right\}. \quad (1.4)$$

Moreover, the function  $v(\rho)$  of (1.1) satisfies

$$v(0) = v_f, \quad v(\rho_{\text{jam}}) = 0.$$

The study of this extended traffic flow system is significant both for practical application and theoretical interest. In real traffic, the drop or increase in traffic capacity that is reflected by  $\theta(x)$  is frequent in many locations, such as on curves and slopes and near ramps and traffic accidents. In particular, by extension  $b_l = b_l(x, t)$  can serve as a switch function in signal traffic or the like (see Section 4.2 for this extension). These changes are usually very sharp, thus, all the coefficients in  $\theta$  are treated as being discontinuous at the change. In other words, the flux  $f(u, \theta(x))$  is a discontinuous function of location  $x$  through the discontinuous function  $\theta(x)$ . When the extension  $b_l = b_l(x, t)$  is considered, the flux  $f(u, \theta(x, t))$  is a discontinuous function of location  $x$  and time  $t$  through the discontinuous function  $\theta(x, t)$ . Another complication comes from the fact that it is usually impossible (for  $m > 2$ ) to solve the eigen-polynomial of system (1.3) explicitly, let alone the solutions to Riemann problems. One would thus be limited to use very crude approximate Riemann solvers such as the Lax–Friedrichs solvers for numerical schemes. Hence, first or even second-order numerical methods will be very dissipative. These together pose significant difficulties for both analytical and numerical studies. See for example [1,2,9,13,14,24–27] for related discussions.

In this paper, some important features of the model are discussed under a modified equivalent system of (1.3), in which all of the components of  $\theta$  are solution variables. Analytically, the hyperbolicity of the system is proven, and the wave-breaking patterns of the Riemann problem are predicted. We note that these descriptions are mostly based on the relevant studies in [24,28]. The maximum absolute value of

all of the eigenvalues is estimated, which is an essential parameter in the proposed numerical schemes. We note that these eigenvalues cannot be explicitly solved (see Section 2 for this discussion).

In developing the numerical schemes, it may not be efficient to apply the standard methods (e.g., TVD, RKDG, and WENO schemes) to system (1.3) directly due to its spatially varying fluxes, especially because the dependency of the flux on the spatial variable  $x$  is discontinuous. It should be mentioned that a wave-propagation method was recently developed that generated good numerical results in solving elastic waves in heterogeneous media, which constitute a  $2 \times 2$  system with spatially varying fluxes [2]. Nevertheless, this method is limited to problems in which an eigenvalue has a fixed sign for all involved  $u$  and  $\theta(x)$ , and requires that the eigenvalues can be solved explicitly. Therefore, this method is not suitable for our problem, in which one of the eigenvalues changes sign, and all are implicit. In [24–27], Zhang et al. developed a numerical scheme to deal with spatially varying fluxes for the scalar case, which can also be extended to the vector case.

With a modified equivalent system of (1.3), a component-wise WENO scheme that applies the Lax–Friedrichs numerical flux in the finite volume method and the flux splitting in the finite difference method are discussed in Section 3. As the modification gives rise to a standard hyperbolic conservation form, the scheme is theoretically sound, and numerically gives good results. Although the Riemann problem of the system generates very complicated wave structures, the numerical results are in good agreement with the claimed wave patterns (Section 4.1). For sharp changes of  $b_l$  from their maxima to minima, which describes the sharp braking of vehicles, the resultant strong discontinuity at the interface is well captured (Section 4.2). We note that this is the first time that the WENO scheme has been applied to hyperbolic conservation laws with spatially varying fluxes. Similar applications to other problems may be possible, which is addressed in Section 5 with several concluding remarks. We also note that, even though the solutions for such traffic flow models have relatively simple structures (almost linear) between discontinuities, the fact that the eigenvalues of the flux Jacobian cannot be obtained explicitly, let alone explicit solutions to the Riemann problems, restricts first and second-order numerical methods to use crude approximate Riemann solvers, such as the Lax–Friedrichs solvers. As a result, first and second-order numerical methods will be very dissipative, and may miss important solution features such as small shocks completely unless an extremely refined mesh is used (see [23] for such an example; see also the last example in Section 4). Therefore, high order WENO schemes as those used in this paper are still good choices to resolve the solution with a coarse mesh to save computational cost.

## 2. Hyperbolicity and wave structure of the model equations

To study the hyperbolicity and solution structure of the system, we rewrite (1.3) in the “standard” conservation form, which means that we add the identity  $\theta_t = 0$  to (1.3). This identity is naturally modified when  $\theta$  depends on  $t$  in the extension in Section 4.2. For convenience, we treat  $\theta$  as a scalar in the following discussions, but the results are equally applicable to the vector case. Accordingly, (1.3) and the added identity can be viewed as the following equivalent  $(m + 1) \times (m + 1)$  system:

$$U_t + F_x = 0, \tag{2.1}$$

where  $U = (u, \theta)^T$  and  $F = (f(u, \theta), 0)^T$ . We note that the construction of equivalent forms of the conservation laws with spatially varying fluxes is widely applied, for example in [1,9,14,25]. According to this standard conservation form, we study the hyperbolicity of the system. We write the Jacobian  $F_U$  and the matrix for solving the eigen-pairs as follows:

$$F_U = \begin{pmatrix} f_u & f_\theta \\ \mathbf{0} & 0 \end{pmatrix}, \quad F_U - \lambda I_{m+1} = \begin{pmatrix} f_u - \lambda I_m & f_\theta \\ \mathbf{0} & -\lambda \end{pmatrix}, \tag{2.2}$$

where  $\mathbf{0} = (0, \dots, 0)$  has  $m$  components,  $f_\theta = (f_{1\theta}, \dots, f_{m\theta})^T$  and  $I_m$  is the  $m \times m$  identity matrix. Let

$$|f_u - \lambda I_m| = P_m(\lambda)$$

and then the eigen-polynomial of  $F_U$  is

$$|F_U - \lambda I_{m+1}| = -\lambda P_m(\lambda). \tag{2.3}$$

*2.1. Hyperbolicity of the model equations*

For the discussed system, it is not difficult to obtain [28]

$$P_m(\lambda) = Q(\lambda) \prod_{l=1}^m (v_l - \lambda), \quad Q(\lambda) = 1 + \sum_{l=1}^m \frac{\rho_l}{v_l - \lambda} \frac{\partial v_l}{\partial \rho}. \tag{2.4}$$

For  $u/a \in D$ , where  $D$  is the open domain that corresponds to  $\bar{D}$  of (1.4), we suppose that  $\{v_l\}_{l=1}^m$  are distinct, namely,

$$v_1 < \dots < v_m, \tag{2.5}$$

then it is easy to verify that, by (2.4),

$$\text{sgn}(P_m(v_l)) = (-1)^l, \quad \text{sgn}\left(P_m\left(v_l + \sum_{l=1}^m \rho_l \frac{\partial v_l}{\partial \rho}\right)\right) = 1. \tag{2.6}$$

By the intermediate value theorem, (2.6) suggests  $m$  distinct real eigenvalues  $\{\lambda\}_{l=1}^m$  of the Jacobian  $f_u$ , which are separated by  $m$  velocities as follows:

$$v_1 + \sum_{l=1}^m \rho_l \frac{\partial v_l}{\partial \rho} < \lambda_1 < v_1 < \lambda_2 < \dots < v_{l-1} < \lambda_l < v_l < \dots < v_{m-1} < \lambda_m < v_m. \tag{2.7}$$

For  $u/a \in \partial D$ ,  $m$  real eigenvalues of  $f_u$  are also ensured, and some inequalities of (2.7) change to equalities. The hyperbolicity of this latter case is rather complicated, but to a degree can be viewed as the limiting case of the former (see [28] for more details). For simplicity, this case is excluded from this section and from Section 2.2.

By (2.3), therefore, we conclude that the Jacobian  $F_u$  has  $m + 1$  real eigenvalues  $\{\lambda_l\}_{l=1}^m$  and  $\tilde{\lambda} = 0$ , and thus that (2.1) is a hyperbolic system. Furthermore, by (2.7) it is obvious that these  $m + 1$  eigenvalues are distinct if and only if  $\lambda_1 \neq \tilde{\lambda} = 0$ , in which case (2.1) is strictly hyperbolic. As is shown in the following, it is possible to have  $\lambda_1 = \tilde{\lambda} = 0$ , in which case system (2.1) is generally non-strictly hyperbolic.

Substituting  $\lambda$  with  $\lambda_1 = 0$  in (2.4) and with all  $v_l$  being given by (1.1), we have

$$Q(0) = \frac{q'(\rho)}{v(\rho)}, \quad \text{sgn}(P_m(0)) = \text{sgn}(q'(\rho)), \tag{2.8}$$

where  $q(\rho) = \rho v(\rho)$ . Usually,  $q(\rho)$  is supposed to be strictly concave [21,23,28],  $q''(\rho) < 0$ . Assume that  $q(\rho^*)$  is the maximum of  $q(\rho)$ , such that

$$q'(\rho^*) = 0, \quad q'(\rho) > 0 \quad \text{for } \rho < \rho^*, \quad q'(\rho) < 0 \quad \text{for } \rho > \rho^*,$$

where  $\rho^*$  is the critical density, as it is called in many traffic flow models. Accordingly, (2.8) and (2.6) give the following conclusion:

$$\lambda_1 \begin{cases} > 0 & \text{if } \rho < \rho^*, \\ = 0 & \text{if } \rho = \rho^*, \\ < 0 & \text{if } \rho > \rho^*. \end{cases} \tag{2.9}$$

This is again derived by the intermediate value theorem.

Suppose that  $(r_l^T, z_l)^T$  is an eigenvector that corresponds to  $\lambda_l$ , where  $r_l$  is a  $m \times 1$  vector and  $z_l$  is a scalar, then we have

$$\lambda = \lambda_l : (F_U - \lambda_l I_{m+1}) \begin{pmatrix} r_l \\ z_l \end{pmatrix} = \begin{pmatrix} f_u - \lambda_l I_m & f_\theta \\ \mathbf{0} & -\lambda_l \end{pmatrix} \begin{pmatrix} r_l \\ z_l \end{pmatrix} = \begin{pmatrix} (f_u - \lambda_l I_m)r_l + z_l f_\theta \\ -\lambda_l z_l \end{pmatrix} = \mathbf{0}.$$

This indicates that we can take  $z_l$  to be zero and  $r_l$  to be the eigenvector of  $f_u$  that corresponds to  $\lambda_l$ .

Suppose that  $(\tilde{r}^T, \tilde{z})^T$  is an eigenvector that corresponds to  $\tilde{\lambda} = 0$ . Similarly, we have

$$\tilde{\lambda} = 0 : (F_U - \tilde{\lambda} I_{m+1}) \begin{pmatrix} \tilde{r} \\ \tilde{z} \end{pmatrix} = \begin{pmatrix} f_u & f_\theta \\ \mathbf{0} & 0 \end{pmatrix} \begin{pmatrix} \tilde{r} \\ \tilde{z} \end{pmatrix} = \begin{pmatrix} f_u \tilde{r} + \tilde{z} f_\theta \\ 0 \end{pmatrix} = \mathbf{0},$$

which implies that  $\tilde{r}$  is the solution of the algebraic equations

$$f_u \tilde{r} = -\tilde{z} f_\theta. \tag{2.10}$$

Denote by  $r = (r_1, \dots, r_m)$  a non-singular matrix of right-eigenvectors of  $f_u$ . The matrix of the right-eigenvectors of  $F_U$  then reads

$$R \equiv \begin{pmatrix} r & \tilde{r} \\ \mathbf{0} & \tilde{z} \end{pmatrix}.$$

If  $\lambda_1 \neq 0$ , then  $f_u$  is non-singular. We choose  $\tilde{z} \neq 0$  in (2.10), and thus  $\tilde{r}$  is uniquely determined as  $\tilde{r} = -\tilde{z} f_u^{-1} f_\theta$ . In this case  $R$  is non-singular and

$$R = \begin{pmatrix} r & -\tilde{z} f_u^{-1} f_\theta \\ \mathbf{0} & \tilde{z} \end{pmatrix}, \quad R^{-1} = \begin{pmatrix} r^{-1} & r^{-1} f_u^{-1} f_\theta \\ \mathbf{0} & 1/\tilde{z} \end{pmatrix}.$$

If  $\lambda_1 = 0$ , then  $f_u$  is singular. Consequently,  $R$  must be singular. This is obvious for  $\tilde{z} = 0$ . For  $\tilde{z} \neq 0$ , if Eq. (2.10) has a solution to  $\tilde{r}$ , then we would read  $\text{rank}(f_u, -\tilde{z} f_\theta) = \text{rank}(f_u) = \text{rank}(f_u - \lambda_1 I_m) = m - 1$ , for which an identity is required. This is generally unlikely under the assumption that  $f_\theta \neq 0$ . For the discussed traffic flow problem, the required identity can be arranged as

$$\sum_{l=1}^m \frac{\partial f_l}{\partial x} \frac{1}{v_l} \equiv 0 \quad \text{or} \quad a \sum_{l=1}^m \frac{b'_l}{b_l} \rho_l - \frac{v'}{v} \rho^2 a' \equiv 0 \quad \text{for } \lambda_1 = 0 \quad \text{or} \quad \rho = \rho^*.$$

However, it is obvious that this condition does not hold for the traffic flow model.

In summary, system (2.1) is strictly hyperbolic for  $\lambda_1 \neq 0$ , but non-strictly hyperbolic for  $\lambda_1 = 0$ .

### 2.2. Wave structure of the model equations

We consider the Riemann problem

$$u = \begin{cases} u^L & \text{if } x < 0, \\ u^{m+1} & \text{if } x > 0, \end{cases} \quad \theta = \begin{cases} \theta^L & \text{if } x < 0, \\ \theta^R & \text{if } x > 0, \end{cases} \tag{2.11}$$

where the expression for  $\theta$  means that  $a(x)$  and  $b(x)$  are discontinuous of  $x$  at the interface, with  $\theta^L = (a^L, b_1^L, \dots, b_m^L)$  and  $\theta^R = (a^R, b_1^R, \dots, b_m^R)$ .

The Riemann problem was solved exactly for a general scalar form of (1.3) ( $m = 1$ ) in [24]. For the case  $m = 2$ ,  $\lambda_1$  and  $\lambda_2$  are explicit, but the solution is very complicated. For  $m > 2$ , no  $\lambda_l$  can be solved explicitly in the discussed traffic flow problem, and thus it is very difficult to derive the analytical results [28]. However, some predictions of the wave structure are possible, because the wave breaking near the interface would be similar to that for the scalar case that is discussed in [24]. Moreover, the monotone changes across or within the waves other than the interface are well understood for the system in which  $\theta(x)$  is constant [28], and these conclusions are still applicable in each of the regions  $D^+ = \{(x,t)|x > 0, t > 0\}$  and  $D^- = \{(x,t)|x < 0, t > 0\}$ . The claimed wave structure in this section serves as a comparison for the numerical results in Section 4.

We call a wave that corresponds to the  $\lambda_l$ - (or  $\tilde{\lambda}$ -) characteristic field the  $\lambda_l$ - (or  $\tilde{\lambda}$ -) wave. In accordance with (2.7), these  $\{\lambda_l\}_{l=2}^m$ -waves must be in the region  $D^+ = \{(x,t)|x > 0, t > 0\}$ , and the  $\tilde{\lambda}$ -wave can be easily verified as a contact at the interface  $x = 0$ . See [10–12,18–20] for detailed accounts of the basic properties of hyperbolic waves. Let  $u^L = u(0^-, t)$  and  $u^R = u(0^+, t)$ , which are, respectively, the left and right solution states that are adjacent to the interface, and we then have, by the Rankine–Hugoniot jump condition,

$$f(u^L, \theta^L) = f(u^R, \theta^R). \tag{2.12}$$

As indicated in [24], the two states  $u^L$  and  $u^R$  should be also “connected” by the  $\lambda_l$  characteristics. This argument implies that the propagation of the  $\lambda_1$ -characteristics may change the angle across the interface, and should satisfy

$$\lambda_1(u^L, \theta^L)\lambda_1(u^R, \theta^R) \geq 0. \tag{2.13}$$

Here, the equality means that  $\lambda_1(u^L, \theta^L)$  or  $\lambda_1(u^R, \theta^R)$  coincides with the contact  $\tilde{\lambda} = 0$ , in which case system (2.1) must be non-strictly hyperbolic. We have, by (2.12),

$$a^L b_l^L \rho_l^L v(\rho^L) = a^R b_l^R \rho_l^R v(\rho^R), \quad l = 1, \dots, m.$$

Let  $\alpha_{1l} = a^L b_l^L / (a^R b_l^R)$  and  $\alpha_{2l} = 1/\alpha_{1l}$ , and the aforementioned equation is then equivalent to

$$\rho_l^R v(\rho^R) = \alpha_{1l} \rho_l^L v(\rho^L) \quad \forall l; \quad \rho^R v(\rho^R) = v(\rho^L) \sum_{l=1}^m \alpha_{1l} \rho_l^L, \tag{2.14}$$

where the second equation is obtained by the summation of the first over  $l$ . Similarly, we obtain

$$\rho_l^L v(\rho^L) = \alpha_{2l} \rho_l^R v(\rho^R) \quad \forall l; \quad \rho^L v(\rho^L) = v(\rho^R) \sum_{l=1}^m \alpha_{2l} \rho_l^R. \tag{2.15}$$

In the discussed traffic flow problem, it is reasonable to assume that

$$\text{if } \alpha_{1k} > 1 \text{ for some } k, \text{ then } \alpha_{1l} \geq 1 \quad \forall l, \tag{2.16}$$

which indicates a non-increase or non-decrease ( $\alpha_{1l} \geq 1$  or  $\alpha_{1l} \leq 1$ ) in traffic capacity for all types of vehicles. Otherwise, the problem would be unrealistic, because the capacity drops for some vehicle types but increases for others in the same location.

Whether system (2.1) is strictly hyperbolic will be subject to (2.13), because  $\theta(x)$  is only changeable across the interface. Let  $u^2$  be the left solution state of the  $\lambda_2$ -wave (Figs. 1 and 2), and we then have the following description.

(1) Suppose that  $\lambda_1(u^L, \theta^L)\lambda_1(u^R, \theta^R) > 0$ , then system (2.1) is strictly hyperbolic and we would expect  $m + 1$  waves. In addition to the  $\tilde{\lambda}$ -contact at the interface, only one  $\lambda_1$ -wave is needed before the  $\lambda_2$ -wave. This  $\lambda_1$ -wave is either in  $D^+$  or  $D^-$  for the consideration of the following three cases:

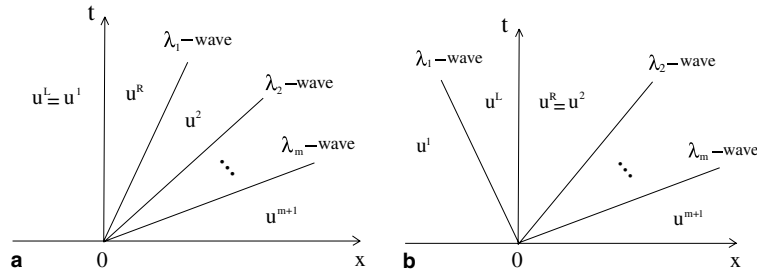


Fig. 1. Wave patterns that correspond to a strictly hyperbolic system (2.1): (a) the  $\lambda_1$ -characteristics pass through the interface from left to right; (b) the  $\lambda_1$ -characteristics pass through the interface from right to left.

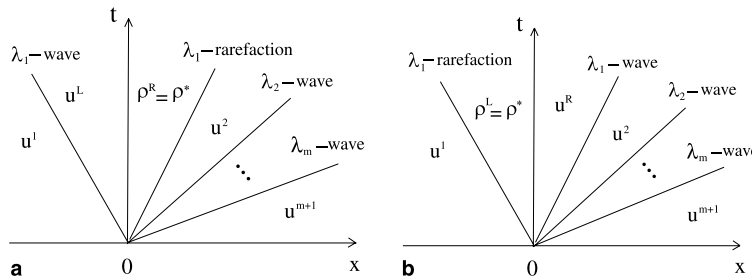


Fig. 2. Wave patterns that correspond to a non-strictly hyperbolic system (2.1): (a) the  $\lambda_1$ -characteristics of  $u = u^1$  are reflected from the interface, forming an extra  $\lambda_1$ -wave in  $D^-$ ; (b) the  $\lambda_1$ -characteristics of  $u = u^2$  are reflected from the interface, forming an extra  $\lambda_1$ -wave in  $D^+$ .

(a) If  $\lambda_1(u^1, \theta^L) > 0$  and  $\lambda_1(u^2, \theta^R) \geq 0$ , then it is natural to have  $u^L = u^1$  and  $\lambda_1(u^L, \theta^L) > 0$ . As  $\lambda_1(u^R, \theta^R) > 0$ , it is inferred by (2.9) that  $\rho^R < \rho^*$ . Such a unique  $\rho^R$  and the components of  $u^R$  are solvable by (2.14) if and only if

$$v(\rho^L) \sum_{l=1}^m \alpha_{1l} \rho_l^L < \rho^* v(\rho^*) = q(\rho^*). \tag{2.17}$$

In this case, we can say that the propagation of  $\lambda_1(u^1, \theta^L)$  is able to pass through the interface and then change to  $\lambda_1(u^R, \theta^R)$ , in which state  $u^R$  forms the  $\lambda_1$ -wave with  $u^2$  in  $D^+$ . Fig. 1(a) shows this wave pattern, where a wave is represented simply by a radial.

(b) If  $\lambda_1(u^1, \theta^L) \leq 0$  and  $\lambda_1(u^2, \theta^R) < 0$ , then similarly we have  $u^R = u^2$  and  $\lambda_1(u^R, \theta^R) < 0$ , and thus  $\lambda_1(u^L, \theta^L) < 0$  and  $\rho^L > \rho^*$ . By (2.15),  $\rho^L$  and  $\{\rho_l^L\}_{l=1}^m$  are uniquely solvable if and only if

$$v(\rho^R) \sum_{l=1}^m \alpha_{2l} \rho_l^R < \rho^* v(\rho^*) = q(\rho^*). \tag{2.18}$$

In this case, we can say that the propagation of  $\lambda_1(u^2, \theta^R)$  is able to pass through the interface and then change to  $\lambda_1(u^L, \theta^L)$ , in which state  $u^L$  forms the  $\lambda_1$ -wave with  $u^1$  in  $D^-$ . This wave pattern is shown in Fig. 1(b).

(c) If  $\lambda_1(u^1, \theta^L) > 0$  and  $\lambda_1(u^2, \theta^R) < 0$ , then we have either  $u^L = u^1$  or  $u^R = u^2$ . Accordingly, the wave pattern is similar to that of 1(a) or (b), as is shown in Fig. 1(a) and (b). We note that at least one of Eqs. (2.14) (with  $u^L = u^1$ ) and (2.15) (with  $u^R = u^2$ ) is solvable, because at least one of the conditions (2.17) (with  $u^L = u^1$ ) and (2.18) (with  $u^R = u^2$ ) must hold under assumption (2.16).



(2) Suppose that  $\lambda(u^L, \theta^L)\lambda(u^R, \theta^R) = 0$ , then system (2.1) is non-strictly hyperbolic and we predict a total of  $m + 2$  waves in the following. For all of the cases under consideration, we need two  $\lambda_1$ -waves that are separated by the interface. This wave structure is also characterized by a  $\lambda_1$ -rarefaction, which is either in  $D^-$  or in  $D^+$ , and is distinguished by two wave patterns that are shown in Fig. 2(a) and (b), respectively.

(a) If  $\lambda_1(u^1, \theta^L) > 0$ ,  $\lambda_1(u^2, \theta^R) \geq 0$ , and (2.17) is not satisfied for  $u^L = u^1$  so that (2.14) is unsolvable (except possibly for  $\rho^R = \rho^*$ ), then by the assumption we can only choose  $\lambda_1(u^R, \theta^R) = 0$ , namely  $\rho^R = \rho^*$ . Moreover, by (2.14) and (2.15), we have

$$v(\rho^L) \sum_{l=1}^m \alpha_{1l} \rho_l^L = \rho^* v(\rho^*) = q(\rho^*), \quad \rho^L v(\rho^L) = v(\rho^*) \sum_{l=1}^m \alpha_{2l} \rho_l^R. \quad (2.19)$$

Comparing the first equation of (2.19) with (2.17), we can see that a maximal principle is applied. The second equation of (2.19) is solvable, because it is implied that  $\alpha_{2l} \leq 1$  ( $\alpha_{1l} \geq 1$ ) for all  $l$ , and thus  $v(\rho^*) \sum_{l=1}^m \alpha_{2l} \rho_l^R \leq v(\rho^*) \rho^* = q(\rho^*)$ . Otherwise, by (2.16), we have  $\alpha_{1l} \leq 1$  for all  $l$ , and (2.17) will be satisfied by  $u^L = u^1$ . However, this contradicts our assumption.

In this case,  $\rho^L$  is chosen such that  $\lambda(u^L, \theta^L) \leq 0$ , namely  $\rho^L \geq \rho^*$ . Therefore, the propagation of  $\lambda_1(u^1, \theta^L)$  is unable to pass through the interface, and reflects backward so that  $u^1$  and  $u^L$  form a  $\lambda_1$ -wave in  $D^-$ . Meanwhile,  $u^R$  and  $u^2$  form another  $\lambda_1$ -wave that can be identified as a rarefaction (see Proposition 2.2), because  $\rho^R = \rho^* > \rho^2$ . This wave pattern is shown in Fig. 2(a).

(b) If  $\lambda_1(u^1, \theta^L) \leq 0$ ,  $\lambda_1(u^2, \theta^R) < 0$ , and (2.18) is not satisfied for  $u^R = u^2$  so that (2.15) is unsolvable (except possibly for  $\rho^L = \rho^*$ ), then we have  $\lambda(u^L, \theta^L) = 0$  or  $\rho^L = \rho^*$ . This case is parallel to 1(a), and the wave structure is shown in Fig. 2(b), where two predicted  $\lambda_1$ -waves are also separated by the interface. In contrast to 2(a), here it is the  $\lambda_1$ -wave in  $D^-$  that is identified as a rarefaction (also see Proposition 2.2), because  $\rho^1 > \rho^L = \rho^*$ .

(c) If  $\lambda_1(u^1, \theta^L) < 0$  and  $\lambda_1(u^2, \theta^R) > 0$ , which suggests that  $\lambda_1(u, \theta)$  changes sign across the interface, then we have  $\lambda_1(u^R, \theta^R) = 0$  for  $\alpha_{1l} \geq 1$ . In this case, the wave structure is similar to that of 2(a), and is also shown in Fig. 2(a). For  $\alpha_{2l} \geq 1$ , we have  $\lambda_1(u^L, \theta^L) = 0$ , and the wave pattern is similar to that of 2(b), as shown in Fig. 2(b). We have the trivial case of this for  $\lambda_1(u^1, \theta^L) = 0$  or  $\lambda_1(u^2, \theta^R) = 0$ .

We note that the inhomogeneity condition makes the breaking of the  $\lambda_1$ -wave unusual in the above. Under the condition that  $\alpha_{1l} \geq 1$  for all  $l$  and  $\alpha_{1k} > 1$  for some  $k$ , the interface actually represents a bottleneck before which an extra  $\lambda_1$ -wave is needed (Fig. 2(a)), provided that the upcoming vehicles are dense enough. Precisely this corresponds to wave patterns 2(a) and (c) with  $\rho^1 \geq \rho^*$  (i.e.,  $\lambda_1(u^1, \theta^L) \leq 0$ ), or the wave pattern 2(a) for which  $\rho^1 < \rho^*$  and  $\rho^2 \geq \rho^*$ , but (2.17) is not satisfied. The latter occurrence is typical of bottleneck traffic for which a “blow-up” in total density ( $\rho^L > \rho^* > \max(\rho^1, \rho^{m+1})$ ) is expected before the interface, corresponding to a  $\lambda_1$ -shock. Under the condition that  $\alpha_{1l} \leq 1$  for all  $l$  and  $\alpha_{1k} < 1$  for some  $k$ , on the other hand, Fig. 2(b) indicates that these denser traffic ( $\rho^1 \geq \rho^*$ ) in wave patterns 2(b) and (c) will be relieved by the  $\lambda_1$ -rarefaction before the interface. Also refer to Propositions 2.1 and 2.2 below.

For the scalar case  $m = 1$ , in which the  $\lambda_l$ -waves disappear for  $l > 1$  and  $u^2 = u^{m+1}$  becomes known initially, the wave patterns as shown in Figs. 1 and 2 are identical to those that were solved exactly and proved to be unique in [24]. The consistency enhances the credibility of the above description of the  $\lambda_1$ -wave that is adjacent to the interface.

Furthermore, the conclusions for all of the  $\lambda_l$ -waves in [28] can be directly applied in this Riemann problem, because each of the waves is either in  $D^-$  or in  $D^+$ , where  $\theta(x)$  is constant. In general, all of these  $\lambda_l$ -characteristic fields are genuinely non-linear, and thus they correspond to either shocks or rarefactions. Let  $u^-$  and  $u^+$  be the left and right states of a certain  $\lambda_l$ -wave, respectively, and, supposing that the function  $v(\rho)$  is concave, namely,  $v''(\rho) \leq 0$ , then the following two propositions in [28] may be cited.



**Proposition 2.1.** A  $\lambda_T$ -shock is characterized by the following:  $\rho^- < \rho^+$ ,  $\rho_k^- < \rho_k^+$  for  $k \geq l$  and  $\rho_k^- > \rho_k^+$  for  $k < l$ .

**Proposition 2.2.** A  $\lambda_T$ -rarefaction is characterized by the following:  $\rho^- > \rho^+$ ,  $\rho_k^- > \rho_k^+$  for  $k \geq l$  and  $\rho_k^- < \rho_k^+$  for  $k < l$ . Moreover, all of the functions  $\rho(\theta)$  and  $\rho_k(\theta)$  are monotone in the rarefaction fan, where  $\theta = x/t$ .

It was also indicated in [28] that the two propositions should be applicable to a generally given function  $v(\rho)$ . Furthermore, the physical meanings of these waves described in the propositions are related to overtaking among all types of vehicles and the wave motions. It was indicated that the  $\lambda_1$ -wave is overtaken by all types of flows. This means that by  $\lambda_1$ -wave the influence on the flow comes from the downstream completely. The  $\lambda_T$ -wave ( $l > 1$ ) is overtaken by the  $k$ th flow for  $k \geq l$ , whereas this wave overtakes the other  $k - 1$  flows. It follows from the above that the  $l$ th flow ( $l < m$ ) is influenced by these  $\lambda_k$  waves both from the downstream (if  $k \leq l$ ) and the upstream (if  $k > l$ ), and that the  $m$ th flow is influenced only by the downstream because it overtakes all other flows. Actually, these conclusions are implied in the inequalities of (2.7) and the monotonicity of all densities as shown in Propositions 2.1 and 2.2 is just for accommodation to the described overtaking. See [28] for more details in the mathematical analysis.

### 3. Numerical schemes

For the numerical approximation of the model equations, we follow the basic ideas that are stated in Section 1. We first apply the modified equivalent system (2.1), which is written in two parts as follows:

$$\begin{aligned} u_t + f(u, \theta)_x &= 0, \\ \theta_t + o_x &= 0, \end{aligned} \tag{3.1}$$

where the flux  $o = 0$ . We note that  $\theta$  is a solution vector for temporal evolution in the computation. Let  $\hat{f}$  and  $\hat{o}$  be the two numerical flux functions that correspond to the fluxes  $f$  and  $o$ , respectively, of (3.1). Then, a standard conservative scheme of (3.1) reads:

$$\begin{aligned} \frac{du_i}{dt} + \frac{1}{\Delta x} (\hat{f}_{i+1/2} - \hat{f}_{i-1/2}) &= 0, \\ \frac{d\theta_i}{dt} + \frac{1}{\Delta x} (\hat{o}_{i+1/2} - \hat{o}_{i-1/2}) &= 0. \end{aligned} \tag{3.2}$$

In the following, the numerical fluxes  $\hat{f}_{i+1/2}$  and  $\hat{o}_{i+1/2}$  are reconstructed by the WENO method through the Lax–Friedrichs flux splitting. As the characteristic decomposition of the system is impossible due to the implicitness of all of the  $\lambda_b$ , or the singularity of the matrix  $R$  that contains the right eigenvectors (see discussions of (2.7)–(2.10)), the component-wise WENO reconstruction is adopted. For a detailed account of the WENO scheme, see [8,15,16] or [23,28], which are more relevant to the discussed model.

#### 3.1. Component-wise finite volume (FV) WENO scheme

The fifth-order accurate WENO FV scheme applies the cell averages  $\{(u_j, \theta_j)\}_{j=i-2}^{i+2}$  to reconstruct  $(u_{i+1/2}^-, \theta_{i+1/2}^-)$ , which are cell boundary values of  $x_{i+1/2}$  on the left-hand side. With  $\{(u_j, \theta_j)\}_{j=i-1}^{i+3}$ ,  $(u_{i+1/2}^+, \theta_{i+1/2}^+)$  are similarly constructed, and are cell boundary values of  $x_{i+1/2}$  on the right-hand side. Thus, we use the Lax–Friedrichs numerical fluxes as follows:

$$\begin{aligned}\hat{f}_{i+1/2} &= \frac{1}{2}(f(u_{i+1/2}^-, \theta_{i+1/2}^-) + f(u_{i+1/2}^+, \theta_{i+1/2}^+) - \alpha(u_{i+1/2}^+ - u_{i+1/2}^-)); \\ \hat{\theta}_{i+1/2} &= -\frac{1}{2}\alpha(\theta_{i+1/2}^+ - \theta_{i+1/2}^-).\end{aligned}\quad (3.3)$$

Eqs. (3.3) and (3.2) constitute a complete semi-discretized scheme.

### 3.2. Component-wise finite difference (FD) WENO scheme

In this scheme, we first use the Lax–Friedrichs flux splitting as follows:

$$\begin{aligned}f^+ &= \frac{1}{2}(f(u, \theta) + \alpha u), \quad f^- = \frac{1}{2}(f(u, \theta) - \alpha u); \\ o^+ &= \frac{1}{2}\alpha\theta, \quad o^- = -\frac{1}{2}\alpha\theta,\end{aligned}\quad (3.4)$$

where  $(u, \theta) = (u_j, \theta_j)$ ,  $j = i - 2, \dots, i + 3$  are point values of the solution. With  $(f_j^+, o_j^+) = (f^+(u_j, \theta_j), o^+(\theta_j)) \equiv w_j$  for  $j = i - 2, \dots, i + 2$ , we proceed with the WENO reconstruction in the cell  $I_i$  to obtain  $w_{i+1/2}^-$ , and then set  $(\hat{f}_{i+1/2}^+, \hat{\theta}_{i+1/2}^+) = w_{i+1/2}^-$ . Similarly, with  $(f_j^-, o_j^-) = (f^-(u_j, \theta_j), o^-(\theta_j)) \equiv w_j$  for  $j = i - 1, \dots, i + 3$ , we proceed with the WENO reconstruction in the cell  $I_{i+1}$  to obtain  $w_{i+1/2}^+$ , and then set  $(\hat{f}_{i+1/2}^-, \hat{\theta}_{i+1/2}^-) = w_{i+1/2}^+$ . The numerical fluxes are thus given by

$$\hat{f}_{i+1/2} = \hat{f}_{i+1/2}^+ + \hat{f}_{i+1/2}^-, \quad \hat{\theta}_{i+1/2} = \hat{\theta}_{i+1/2}^+ + \hat{\theta}_{i+1/2}^-. \quad (3.5)$$

Eqs. (3.5) and (3.2) give the scheme.

In (3.3) and (3.4),  $\alpha \equiv \max_{(u, \theta)} \max_{1 \leq l \leq m} |\lambda_l(u, \theta)|$ . As all of the  $\lambda_l$  are implicit, a slightly larger estimation of  $\alpha$  is made according to (2.7)

$$\alpha = \max_{(u, \theta)} \max \left( \left| v_1 + \sum_{l=1}^m \rho_l \frac{\partial v_l}{\partial \rho} \right|, |v_m| \right). \quad (3.6)$$

The maximum is taken over the relevant region of  $(u, \theta) = (u_j, \theta_j)$  for all  $j$ .

We apply the third-order accurate TVD Runge–Kutta time discretization [17], for which the semi-discrete scheme (3.2) is written as the ODEs

$$u_t = L(u, \theta).$$

For the numerical stability of the described WENO scheme, considerable numerical experience suggests the following CFL condition [6]:

$$\alpha^{(n)} \frac{\Delta t^{(n)}}{\Delta x} \leq \text{CFL}, \quad (3.7)$$

where the CFL number can be taken as 0.6, and  $\Delta t^{(n)}$  and  $\alpha^{(n)}$  are the corresponding values at time level  $n$ . It is favorable that the same CFL condition is also applicable even though the inhomogeneous factors are included in the model.

With respect to the discussed schemes, we remark that the application of the Lax–Friedrichs flux splitting is crucial because it generates correct numerical viscosity that follows the characteristic direction and stabilizes the shock profile. Under the standard conservative scheme of the form (3.2), which corresponds to the standard conservation form (3.1), the numerical viscosity is represented (taking the FV scheme for example) by  $-0.5\alpha(u_{i+1/2}^+ - u_{i+1/2}^-)$  and  $-0.5\alpha(\theta_{i+1/2}^+ - \theta_{i+1/2}^-)$  in (3.3). This is theoretically sound provided that the system is strictly hyperbolic (Fig. 1 and the corresponding wave patterns 1(a)–(c)); moreover, it also performs well according to our numerical test even for non-strictly hyperbolic cases (Fig. 2 and the

corresponding wave patterns 2(a)–(c)). The Roe flux splitting appears to be another simple choice but it is likely to generate entropy violating solution [16].

On the other hand, the first-order Lax–Friedrichs scheme generates too much numerical viscosity which smoothes discontinuities considerably. To retrieve a sharp profile, as usual the WENO reconstruction is adopted because of its high-resolution and higher-order accuracy, which suppresses non-physical oscillations at the same time. In addition, the WENO scheme can be easily implemented without the designing of limiters [16]. Of course, a well estimated viscous coefficient  $\alpha$  by (2.7) is also extremely important in reducing redundant numerical viscosity so as to improve a discontinuous profile.

We note that a direct application of the scheme to original conservation form (1.3) is to drop the second equality of (3.1), and thus these second equalities of (3.2)–(3.4). This naturally suggests that the discontinuous coefficients in  $\theta(x)$  be fixed for temporal evolution, as they appear to be. However, significant numerical oscillations appear near the interface (the discontinuity of  $\theta$ ) in our numerical test.

Finally, numerical experiment indicates that the replacement of the Lax–Friedrichs flux with the local Lax–Friedrichs flux in our schemes of (3.2)–(3.6) makes little difference in numerical results. Here, the local Lax–Friedrichs flux is different from the (global) Lax–Friedrichs flux only by the maximum in (3.6) which is taken over  $j = i - 2, \dots, i + 3$ . Accordingly, the viscosity coefficient is denoted by  $\alpha = \alpha_i$  and  $\alpha^{(n)}$  of (3.7) is the maximum taken over all  $i$ .

#### 4. Numerical examples

In Section 4.1, numerical tests are conducted to determine the waves that are described in Section 2.2. The traffic that approaches the stop line of a traffic signal is simulated in Section 4.2. These examples are computed using the component-wise FD WENO scheme. We note that the component-wise FV WENO scheme generates similar results.

For a clear observation of these waves, the velocities of (1.1) are set to be linear [7,22],

$$v(\rho) = v_f \left( 1 - \frac{\rho}{\rho_{\text{jam}}} \right).$$

In all of the illustrations, the densities  $\rho_l$  and  $\rho$  are scaled by  $\rho_{\text{jam}}$  so that  $0 \leq \rho_l, \rho \leq 1$ , and the spatial and temporal lengths  $L$  and  $T$  of the computational domain  $(0, L) \times (0, T)$  are scaled to unity. These dimensionless variables are also used wherever they are not followed by a unit.

##### 4.1. Resolution of the waves compared to the analytical results

The initial data in this section are given by the Riemann problem (2.11), with the translation of  $x = 0$  to  $x = x_0$  somewhere in  $(0, L)$ . Furthermore, we set  $m = 3$ , which is small enough for a clear observation of the wave breaking. For simplicity,  $b_l(x)$  are set to be constant for all  $l$ , namely,

$$b_1(x) = 0.5, \quad b_2(x) = 0.75, \quad b_3(x) = 1. \tag{4.1}$$

The other parameters are:

$$L = 8000 \text{ m}, \quad T = 400 \text{ s}, \quad v_f = 20 \text{ m/s}, \quad \Delta x = 10 \text{ m}, \quad \text{and} \quad \Delta t^{(n)} = 0.6 \Delta x / \alpha^{(n)},$$

where  $T$  is the simulation time.

Figs. 3–10 show the numerical results, which are designed to reproduce all of the analytical wave patterns in Section 2.2, and to confirm Propositions 2.1 and 2.2. In each figure, we observe the waves as follows.

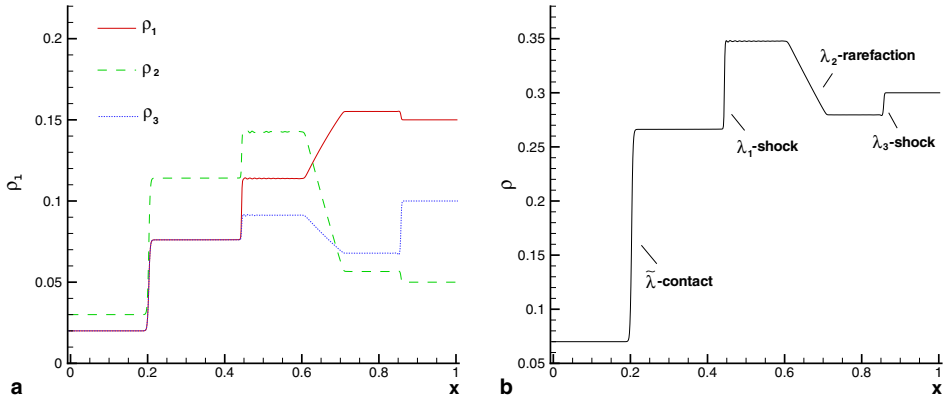


Fig. 3. Wave pattern 1(a) with  $x_0 = 0.2$ ,  $a^L = 3$ ,  $a^R = 1$ ,  $u^l/a^L = (0.02, 0.03, 0.02)^T$ , and  $u^{m+1}/a^R = (0.15, 0.05, 0.1)^T$  as compared with Fig. 1(a): (a) density  $\rho_i$ ; (b) total density  $\rho$ .

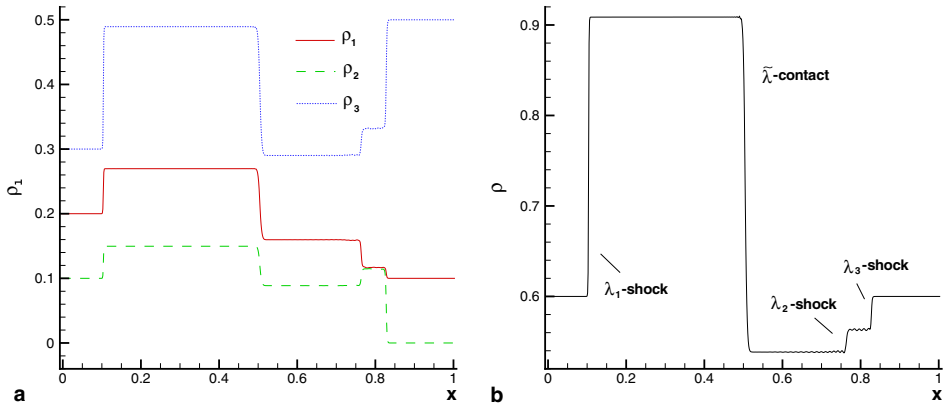


Fig. 4. Wave pattern 1(b) with  $x_0 = 0.5$ ,  $a^L = 3$ ,  $a^R = 1$ ,  $u^l/a^L = (0.2, 0.1, 0.3)^T$ , and  $u^{m+1}/a^R = (0.1, 0, 0.5)^T$  as compared with Fig. 1(b): (a) density  $\rho_i$ ; (b) total density  $\rho$ .

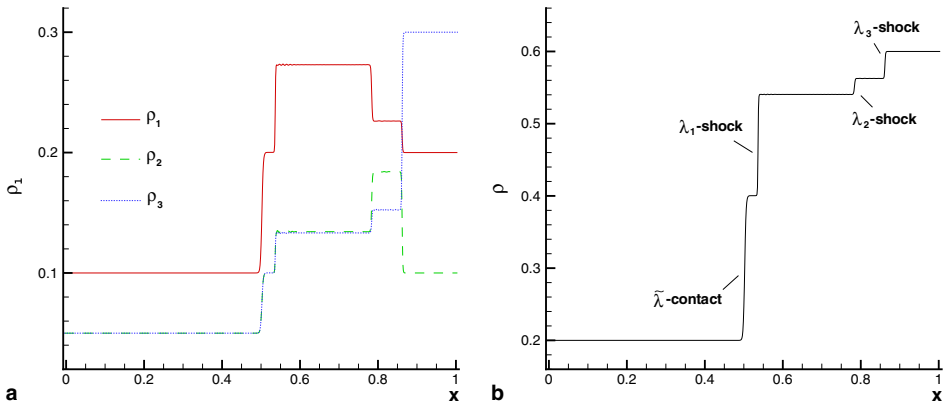


Fig. 5. Wave pattern 1(c) with  $x_0 = 0.5$ ,  $a^L = 3$ ,  $a^R = 2$ ,  $u^l/a^L = (0.1, 0.05, 0.05)^T$ , and  $u^{m+1}/a^R = (0.2, 0.1, 0.3)^T$  as compared with Fig. 1(a): (a) density  $\rho_i$ ; (b) total density  $\rho$ .

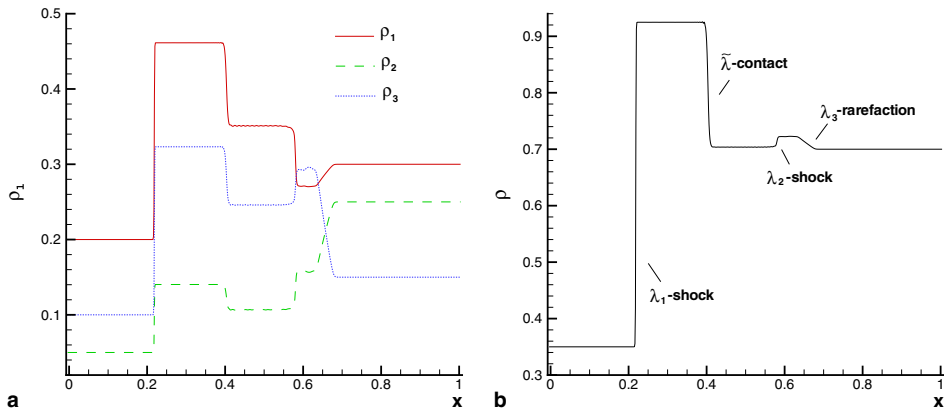


Fig. 6. Wave pattern 1(c) with  $x_0 = 0.4$ ,  $a^L = 3$ ,  $a^R = 1$ ,  $u^1/a^L = (0.2, 0.05, 0.1)^T$ , and  $u^{m+1}/a^R = (0.3, 0.25, 0.15)^T$  as compared with Fig. 1(b): (a) density  $\rho_i$ ; (b) total density  $\rho$ .

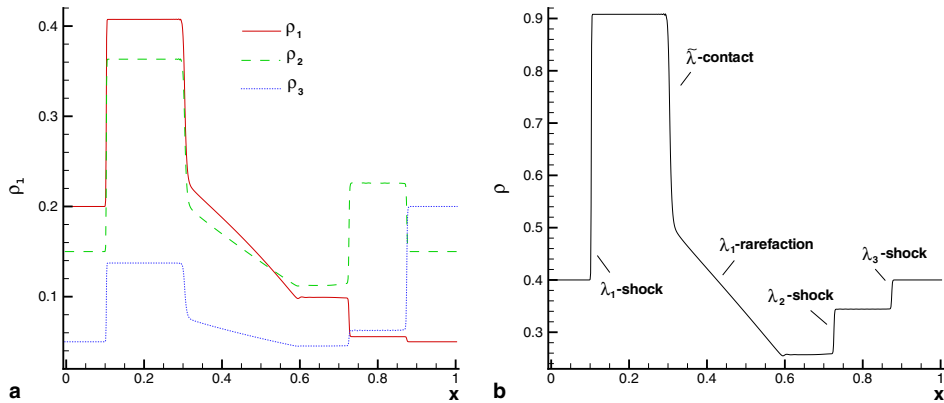


Fig. 7. Wave pattern 2(a) with  $x_0 = 0.3$ ,  $a^L = 3$ ,  $a^R = 1$ ,  $u^1/a^L = (0.2, 0.15, 0.05)^T$ , and  $u^{m+1}/a^R = (0.05, 0.15, 0.2)^T$  as compared with Fig. 2(a): (a) density  $\rho_i$ ; (b) total density  $\rho$ .

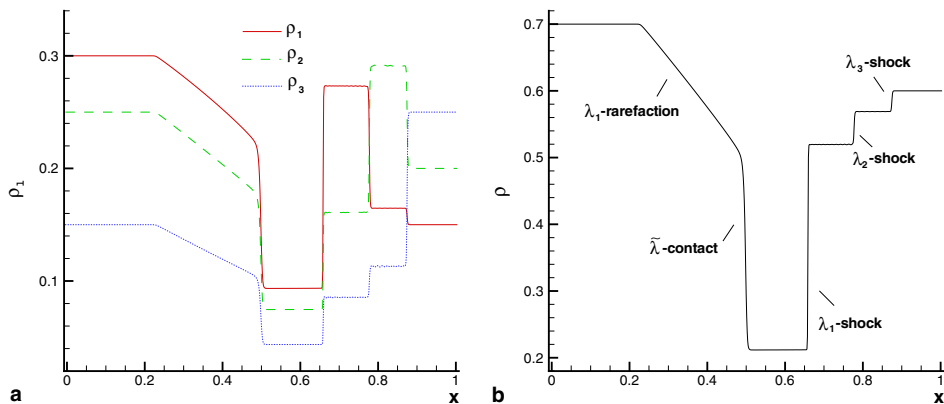


Fig. 8. Wave pattern 2(b) with  $x_0 = 0.5$ ,  $a^L = 2$ ,  $a^R = 3$ ,  $u^1/a^L = (0.3, 0.25, 0.15)^T$ , and  $u^{m+1}/a^R = (0.15, 0.2, 0.25)^T$  as compared with Fig. 2(b): (a) density  $\rho_i$ ; (b) total density  $\rho$ .

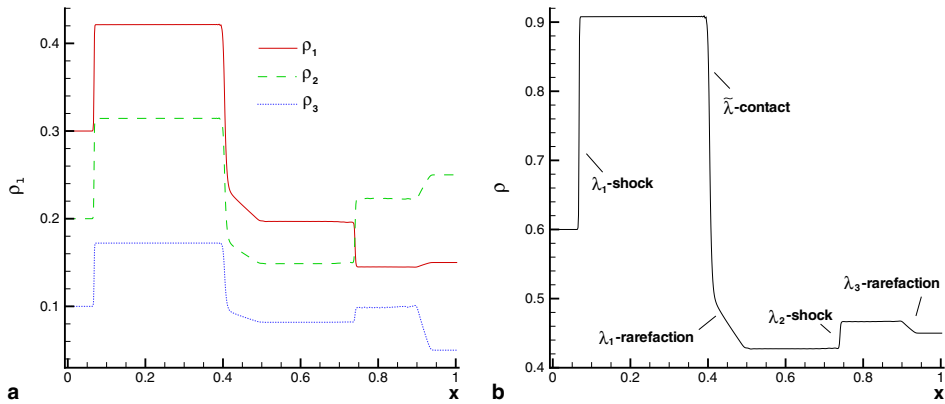


Fig. 9. Wave pattern 2(c) with  $x_0 = 0.4$ ,  $a^L = 3$ ,  $a^R = 1$ ,  $u^l/a^L = (0.3, 0.2, 0.1)^T$ , and  $u^{m+1}/a^R = (0.15, 0.25, 0.05)^T$  as compared with Fig. 2(a): (a) density  $\rho_i$ ; (b) total density  $\rho$ .

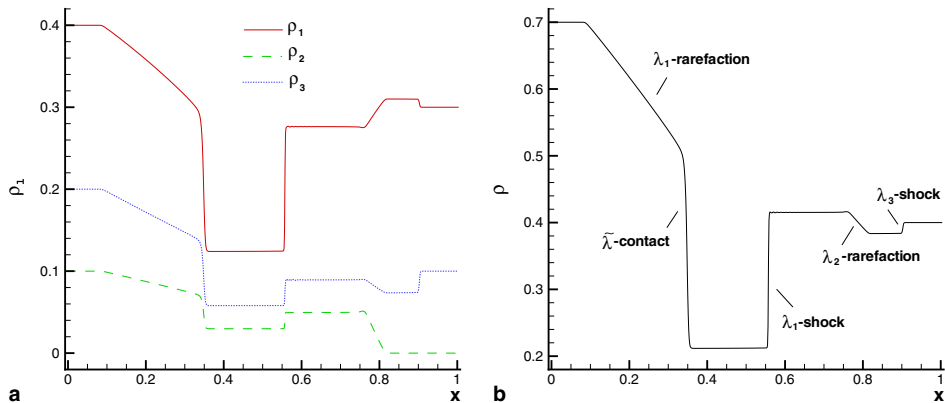


Fig. 10. Wave pattern 2(c) with  $x_0 = 0.35$ ,  $a^L = 2$ ,  $a^R = 3$ ,  $u^l/a^L = (0.4, 0.1, 0.2)^T$ , and  $u^{m+1}/a^R = (0.3, 0, 0.1)^T$  as compared with Fig. 2(b): (a) density  $\rho_i$ ; (b) total density  $\rho$ .

First, we count the wave number. Four  $(m + 1)$  waves are observed in Figs. 3–6 that correspond to the wave patterns that are described in 1(a)–(c) and illustrated in Fig. 1(a) and (b). In these cases, the system is strictly hyperbolic. In Figs. 7–10, there are five  $(m + 2)$  waves, which correspond to the wave patterns that are described in 2(a)–(c) and illustrated in Fig. 2(a) and (b). In these cases, the system must be non-strictly hyperbolic.

Second, we identify all of the  $\lambda_i$ -waves in each figure according to Propositions 2.1 and 2.2. We first observe the monotone change of the total density that is shown in the right part of the figure, such that each of these waves is identified to be either a shock or a rarefaction. Accordingly, as shown in the left part of the figure, the monotone changes for all density  $\rho_i$  across or in the same wave are observed and confirmed to be in accordance with Proposition 2.1 (for a shock) or Proposition 2.2 (for a rarefaction).

Third, as shown in Figs. 7(b)–10(b), we note that  $\rho^R = \rho^* = 0.5$  (in Figs. 7(b) and 9(b)) or  $\rho^L = \rho^* = 0.5$  (in Figs. 8(b) and 10(b)) for the  $\lambda_1$ -rarefaction. These are the analytical results of the wave breaking across the interface ( $\tilde{\lambda}$ -contact).

a

b

c

Fig. 11. Traffic states during a signal cycle that is controlled by (4.2). The initial data are given by (4.3) and the other parameters are  $\Delta x = 1.5$  m and  $\Delta t^{(n)} = 0.3\Delta x/v^{(n)}$ . (a) Densities of all classes at  $t = 30$  s; (b) total density at  $t = 30$  s; (c) change of total density for the simulation time  $T = 60$  s.



For the initial condition:

$$u(x, 0)/a = (0.05, 0.25, 0.05)$$

the numerical result is shown in Fig. 12. A shock line, which propagates to the right, is observed. The density  $\rho$  reaches its maximum value at the shock. A shock is observed with a long period of overtaking between the three vehicles in a period when the queueing is able to simulate traffic signals.

To test the adaptability of the model to different vehicle types, we also set  $m = 5$

$$(b_1, b_2, b_3, b_4, b_5) = \left\{ \begin{array}{l} (0.05, 0.25, 0.05) \\ (0.05, 0.25, 0.05) \end{array} \right.$$

The initial data are given by

$$u(x, 0)/a = (0.15, 0.05, 0.05)$$

The change in total density function in this example is that predicted by the model.

Finally, we remark that the total density function varies spatially and temporally. The change in total density function at each step for temporal update is taken as the new initial condition. This would make no difference to the results. The intervals between temporal updates are variable. Actually all the coefficients are constant with long intervals near the shock. On the other hand, the intervals are small near the shock.  $\theta = \theta(x, t)$ .

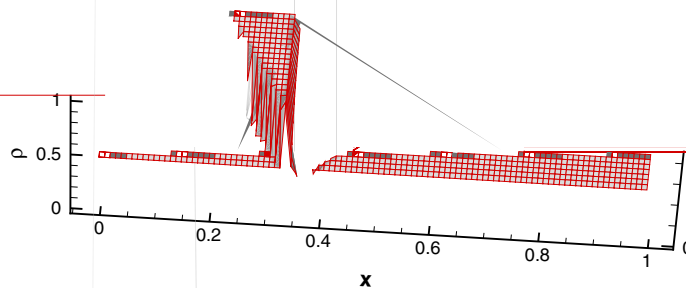


Fig. 12. Change of total density for the simulation time  $T = 60$  s during a signal cycle that is controlled by (4.4). The initial data are given by (4.5) and the other parameters are  $\Delta x = 1.5$  m and  $\Delta t^{(n)} = 0.3\Delta x/\alpha^{(n)}$ .

## 5. Conclusion

With the modified system, this numerical test of the multi-class traffic flow model on an inhomogeneous highway shows the robustness of the WENO reconstruction when combined with the Lax–Friedrichs flux splitting or Lax–Friedrichs numerical flux. Based on this standard hyperbolic conservation system (despite it being non-strictly hyperbolic), the Lax–Friedrichs flux gives correct numerical viscosity for the convergence of the numerical solutions to physically relevant solutions, whereas the WENO reconstruction reduces the surplus numerical viscosity to achieve a high level of resolution of the claimed waves. This again indicates the robustness of the WENO reconstruction, especially when it is combined with the Lax–Friedrichs flux to solve many complexities in application problems.

The application of the WENO scheme in this paper can be extended to solve other hyperbolic conservation laws with spatially varying fluxes, such as elastic waves in heterogeneous media. It would also be interesting to investigate the use of other well-known numerical schemes, such as the RKDG scheme [4,5,3].

## Acknowledgments

The work described in this paper was jointly supported by grants from the Hong Kong Research Grants Council of the Hong Kong Special Administrative Region, China (Project No. HKU 7031/02E) and the National Natural Science Foundation of China (Project No. 10472064). The research of the third author was also supported by NSF Grant DMS-0207451 and ARO Grant W911NF-04-1-0291.

## References

- [1] P. Baiti, H.K. Jenssen, Well-posedness for a class of  $2 \times 2$  conservation laws with  $L_\infty$  data, *Journal of Differential Equations* 140 (1997) 161–185.
- [2] D.B. Bale, R.J. LeVeque, S. Mitran, A. Rosmanith, A wave propagation method for conservation laws and balance laws with spatially varying flux functions, *SIAM Journal of Scientific Computing* 24 (2002) 955–978.
- [3] B. Cockburn, An introduction to the discontinuous Galerkin method for convection-dominated problems, in: B. Cockburn, C. Johnson, C.-W. Shu, E. Tadmor (Eds.), *Advanced Numerical Approximation of Nonlinear Hyperbolic Equations*, in: A. Quarteroni (Ed.), *Lecture Notes in Mathematics*, vol. 1697, Springer, New York, 1998, pp. 151–268.
- [4] B. Cockburn, C.-W. Shu, TVB Runge–Kutta local projection discontinuous Galerkin finite element method for conservation laws II: general framework, *Mathematics of Computation* 52 (1989) 411–435.
- [5] B. Cockburn, C.-W. Shu, The Runge–Kutta local projection  $P$ -discontinuous Galerkin methods for scalar conservation laws, *Modelisation Mathematique et Analyse Numerique* 25 (1991) 337–361.
- [6] S. Gottlieb, C.-W. Shu, E. Tadmor, Strong stability preserving high order time discretization method, *SIAM Review* 43 (2001) 89–112.
- [7] B.D. Greenshields, An analysis of traffic flow, *Proceedings of the Highway Research Board* 14 (1934) 448–477.
- [8] G. Jiang, C.-W. Shu, Efficient implementation of weighted ENO schemes, *Journal of Computational Physics* 126 (1996) 202–228.
- [9] R.A. Klausen, Stability of conservation laws with discontinuous coefficients, *Journal of Differential Equations* 157 (1999) 41–60.
- [10] P.D. Lax, Hyperbolic systems of conservation laws II, *Communications on Pure and Applied Mathematics* 10 (1957) 537–566.
- [11] P.D. Lax, Shock waves and entropy, in: *Contributions to Nonlinear Functional Analytical Proceedings Symposium at the University of Wisconsin*, 1971, p. 603.
- [12] P.D. Lax, *Hyperbolic Systems of Conservation Laws and the Mathematical Theory of Shock Waves*, SIAM, Philadelphia, 1973.
- [13] R.J. LeVeque, Finite-volume methods for non-linear elasticity in heterogeneous media, *International Journal for Numerical Methods in Fluids* 40 (2002) 93–104.
- [14] L. Lin, J.B. Temple, J. Wang, Suppression of oscillations in Godunov’s method of a resonant non-strictly hyperbolic system, *SIAM Journal of Numerical Analysis* 32 (1995) 841–864.
- [15] X.-D. Liu, S. Osher, T. Chan, Weighted essentially nonoscillatory schemes, *Journal of Computational Physics* 115 (1994) 200–212.

- [16] C.-W. Shu, Essentially non-oscillatory and weighted essentially non-oscillatory schemes for hyperbolic conservation laws, in: B. Cockburn, C. Johnson, C.-W. Shu, E. Tadmor (Eds.), *Advanced Numerical Approximation of Nonlinear Hyperbolic Equations*, in: A. Quarteroni (Ed.), *Lecture Notes in Mathematics*, vol. 1697, Springer, New York, 1998, pp. 325–432.
- [17] C.-W. Shu, S. Osher, Efficient implementation of essentially non-oscillatory shock-capturing schemes, *Journal of Computational Physics* 77 (1988) 439–471.
- [18] J. Smoller, *Shock Waves and Reaction–Diffusion Equations*, Springer-Verlag, New York, 1994.
- [19] E.F. Toro, *Riemann Solvers and Numerical Methods for Fluid Dynamics*, Springer-Verlag, New York, 1999.
- [20] G.B. Whitham, *Linear and Nonlinear Waves*, Wiley, New York, 1974.
- [21] G.C.K. Wong, S.C. Wong, A multi-class traffic flow model – an extension of LWR model with heterogeneous drivers, *Transportation Research* 36A (2002) 827–841.
- [22] S.C. Wong, G.C.K. Wong, An analytical shock-fitting algorithm for LWR kinematic wave model embedded with linear speed–density relationship, *Transportation Research* 36B (2002) 683–706.
- [23] M.P. Zhang, C.-W. Shu, G.C.K. Wong, S.C. Wong, A weighted essentially non-oscillatory numerical scheme for a multi-class Lighthill–Whitham–Richards traffic flow model, *Journal of Computational Physics* 191 (2003) 639–659.
- [24] P. Zhang, R.X. Liu, Hyperbolic conservation laws with space-dependent flux: I Characteristics theory and Riemann problem, *Journal of Computational and Applied Mathematics* 156 (2003) 1–21.
- [25] P. Zhang, R.X. Liu, Hyperbolic conservation laws with space-dependent flux: II General study on numerical fluxes, *Journal of Computational and Applied Mathematics* 176 (2005) 105–129.
- [26] P. Zhang, R.X. Liu, Generalization of Runge–Kutta discontinuous Galerkin method to LWR traffic flow model with inhomogeneous road conditions, *Numerical Methods for Partial Differential Equations* 21 (2005) 80–88.
- [27] P. Zhang, R.X. Liu, S.C. Wong, High-resolution numerical approximation of traffic flow problems with variable lanes and free flow velocities, *Physical Review E* 71 (2005) 056704.
- [28] P. Zhang, R.X. Liu, S.C. Wong, S.Q. Dai, Hyperbolicity and kinematic waves of a class of multi-population partial differential equations, *European Journal of Applied Mathematics*, in press.